EJN European Journal of Neuroscience

FENS Federation of European Neuroscience Societies

European Journal of Neuroscience, Vol. 39, pp. 1943–1950, 2014 doi:10.1111/ejn.12614

Spike detection from noisy neural data in linear-probe recordings

Takashi Takekawa,[1,2] Keisuke Ota,[3] Masanori Murayama[3] and Tomoki Fukai[2]
[1]Faculty of Informatics, Kogakuin University, 1-24-2 Nishi-Shinjuku, Shinjuku, Tokyo 163-8677, Japan
[2]Laboratory for Neural Circuit Theory, RIKEN Brain Science Institute, 2-1 Hirosawa, Wako, Saitama 351-0198, Japan
[3]Behavioral Neurophysiology Laboratory, RIKEN Brain Science Institute, Wako, Saitama, Japan

Keywords: diversified spike waveforms, error rate estimation, mouse, multi-electrode, peak distribution

Abstract

Simultaneous recordings of multiple neuron activities with multi-channel extracellular electrodes are widely used for studying information processing by the brain's neural circuits. In this method, the recorded signals containing the spike events of a number of adjacent or distant neurons must be correctly sorted into spike trains of individual neurons, and a variety of methods have been proposed for this spike sorting. However, spike sorting is computationally difficult because the recorded signals are often contaminated by biological noise. Here, we propose a novel method for spike detection, which is the first stage of spike sorting and hence crucially determines overall sorting performance. Our method utilizes a model of extracellular recording data that takes into account variations in spike waveforms, such as the widths and amplitudes of spikes, by detecting the peaks of band-pass-filtered data. We show that the new method significantly improves the cost–performance of multi-channel electrode recordings by increasing the number of cleanly sorted neurons.

Introduction

Functions of the brain emerge essentially from the orchestrated activation of many neurons in neuronal networks. Optical recordings, typically calcium imaging, are advantageous over electrophysiological recordings in the simultaneous recording of very many neurons and in the identification of the cell types of recorded neurons. However, the validity of such methods is restricted by the low temporal resolution (~ several hundreds of milliseconds) of recorded signals, and the reliable detection of single spikes is technically challenging. In contrast, extracellular recordings with multi-channel electrodes allow us to observe neural population activity with a high temporal resolution of millisecond range. Although multi-unit recordings cannot reliably identify the cell types, the fine temporal resolution makes the method particularly useful for studying the spiking dynamics of a neural population.

A technical challenge in multi-neuron recordings is a reliable separation of spikes belonging to the individual neurons from the recorded signals, which contain spikes of many neurons around the electrode. Several methods, including our own (Takekawa *et al.*, 2010, 2012), have been proposed for spike sorting (Hulata *et al.*, 2002; Pouzat *et al.*, 2002; Shoham *et al.*, 2003; Quian Quiroga *et al.*, 2004; Zhang *et al.*, 2004). Spike sorting in general consists of three steps, i.e. the detection of spikes from the raw data, the extraction of characteristic features of the detected spikes, and the clustering of spikes belonging to different neurons based on the extracted features (Schmidt, 1984; Lewicki, 1998). For instance, in our previous methods, feature extraction was performed based on principal component analysis of the multimodality of distributions, and spike clustering was formulated based on the variational Bayes method. These algorithms are implemented using open software, EToS1 and EToS3 (http://etos.sourceforge.net/), and EToS3 has been widely appreciated as a high-performance spike sorting system.

However, the previous methods have difficulty in parameter setting and the detection of spikes when spike waveforms are non-stationary and/or of low amplitude. Because the spatial distance between the electrode and a recorded neuron varies, the amplitude of the recorded spike waveforms varies significantly. In addition, the widths of spikes vary from neuron to neuron because the recorded neuron group generally contains multiple cell types. The frequency of spike firing also varies from neuron to neuron, implying that the number of spike samples differs for different neurons. In fact, the previous methods could not isolate many neurons if neuronal firing is sparse and the number of spike samples is limited. Here we propose a novel method for spike detection that considers all the above difficulties. This method can efficiently detect spikes with small amplitudes to increase the number of spike samples. We show the virtues of the method using artificial data and extracellular recording data recorded with a linear probe. The proposed method can be combined with a broad class of methods for feature extraction and spike clustering (Quian Quiroga *et al.*, 2004; Zhang *et al.*, 2004; Ghanbari *et al.*, 2011).

Correspondence: Drs T. Fukai, T. Takekawa, [2]Laboratory for Neural Circuit Theory, and [1]Faculty of Informatics, as above.
E-mails: tfukai@riken.jp; takekawa@cc.kogakuin.ac.jp

Received 5 January 2014, revised 4 April 2014, accepted 6 April 2014

Materials and methods

Model of extracellular recording data

We assume that an observed data point x at time t arises from sparse positive signal s (spikes) with additive noise $\varepsilon : x(t) = s(t) + \varepsilon(t)$, where $s(t) = 0$ if no spikes exist at that time. The distribution of data points across time bins is then described as the following sum: $p(x) = p(x, s > 0) + p(x, s = 0)$. Throughout this paper, the amplitudes of simulated data are shown in arbitrary units although in reality they are in the range of several tens of microvolts. We estimate the probability $P(s > 0|x) = p(x, s > 0)/p(x)$ that an observed datum x belongs to a spike, where the equality follows from Bayes theorem. To this end, we estimate the number of true positive (TP) and false positive (FP) signals in the spikes detected with threshold X as follows: $N_{\mathrm{TP}} = N\int_X^\infty p(x, s > 0)\mathrm{d}x$ and $N_{\mathrm{FP}} = N - N_{\mathrm{TP}}$, where N is the total number of detected signals. Then, the number of TP signals in observed data $\{x_i\}$ can be evaluated as $N_{\mathrm{TP}} = \sum_{x_i \geq X} P(s > 0|x_i)$, using $N_{\mathrm{TP}} = N\int_X^\infty p(x)P(s > 0|x)\mathrm{d}x$.

Note that the value of X remains arbitrary and we want to determine it according to a reasonable criterion. Although other choices may be also useful, we determine the value of the threshold by maximizing $N_{\mathrm{TP}} - N_{\mathrm{FP}}$ with respect to X. From the above expression of N_{TP}, we can show that this occurs when $N'_{\mathrm{TP}} = N'_{\mathrm{FP}}$, or $P\ (s > 0|x) = 1/2$, where the prime means derivative with respect to X. Therefore, this criterion implies that the probability that a data point x represents a spike is 1/2 at the threshold.

Delta-function spike model

Previously, Nenadic & Burdic (2005) considered a model in which signals are represented by delta-function-like spikes occurring with a fixed amplitude λ according to the following probability distribution (Nenadic & Burdic, 2005):

$$p_\delta(s) = r\,\delta(s - \lambda) + (1 - r)\delta(s), \qquad (0 \leq r \leq 1) \tag{1}$$

where $\delta(x)$ is Dirac's delta function (see Fig. 1a and b). Then, because $x = s + \varepsilon$, if ε is Gaussian white noise with mean μ and variance σ^2 (see Fig. 1c and d), we can represent the probability distribution function of observed data points x as

$$p_\delta(x) = r\mathcal{N}\left(x\middle|\mu + \lambda, \sigma^2\right) + (1 - r)\mathcal{N}\left(x\middle|\mu, \sigma^2\right). \tag{2}$$

Then, by estimating the values of parameters μ, σ, λ and r from the observed data, we may derive the optimum value of threshold X_δ as

$$X_\delta = \arg\max_X \left[N_{\delta,\mathrm{TP}}(X) - N_{\delta,\mathrm{FP}}(X)\right] = \mu + \frac{\lambda}{2} + \frac{\sigma^2}{\lambda}\log\frac{1 - r}{r}, \tag{3}$$

from the condition $N'_{\mathrm{TP},\delta} - N'_{\mathrm{FP},\delta} = p(x, s > 0) - p(x, s = 0) = 0$, or

$$r\mathcal{N}\left(x\middle|\mu + \lambda, \sigma^2\right) - (1 - r)\mathcal{N}\left(x\middle|\mu, \sigma^2\right) = 0. \tag{4}$$

Finite-width spike model

The above approach does not take into account either the width of spikes or possible variations in signal amplitudes. In fact, extracellular recording data generally contain signals with various amplitudes, including very weak ones (see Fig. 1f and g). It is therefore unlikely that a mixture of two Gaussians accurately describes the probability distribution function of x.

Therefore, we propose a novel model of extracellular recording data to estimate the optimum threshold when spikes have finite widths (or duration) and variable amplitudes. The proposed method has four steps: (1) band-pass filtering of the observed data; (2) detection of the temporal location of positive peaks in the filtered data; (3) estimation of parameters for the distribution of the peaks; and (4) derivation of an appropriate threshold from the model. The first step is necessary to remove high-frequency noise from the data. The second step is crucial for avoiding the difficult estimation of the distribution of the filtered data over time when spike waveforms may vary in an unknown manner. Thus, the amplitudes of peak z are distributed in the filtered data according to

$$p_w(z) = \frac{r}{\sigma}X\left(\frac{z - \mu - \lambda}{\sigma}\right) + \frac{1 - r}{\sigma}Y\left(\frac{z - \mu}{\sigma}\right), \tag{5}$$

where $X(\eta)$ is the distribution of normalized Gaussian white noise $\eta(t)$ after filtering, and $Y(\eta)$ is the distribution of the peak amplitudes of this filtered normalized noise. In short, the first term represents contributions from signals, in which z is distributed around $\mu + \lambda$, and the second term represents contributions from the peaks of noise. In this study, we use the numerical tables of X and Y calculated for $\eta(t)$. Then, as in Eqn (2), we have to estimate the values of four parameters, μ, σ, λ and r, in Eqn (5), implying that the finite-width model is computationally as economical as the delta-function model.

Finite-width variable-amplitude spike model

Finally, we present a model in which the amplitude of finite-width spikes varies from time to time. Unless otherwise stated, we use this model in this study. Note that, due to the presence of noise, a true spike may not give a peak of the observed data when the amplitude is very small. Roughly speaking, this occurs when the amplitude of a spike is overwhelmed by that of noise. Therefore, we estimate the probability of detecting a spike with normalized amplitude $a = \lambda/\sigma$ as erf = (βa) in terms of the error function and a positive constant β. Then, Eqn (5) can be rewritten as

$$p_{\mathrm{aw}}(z) = \frac{r}{\sigma}A\left(\frac{z - \mu}{\sigma}\right) + \frac{1 - r}{\sigma}Y\left(\frac{z - \mu}{\sigma}\right), \tag{6}$$

where the signal contributions should be replaced with

$$A(\eta) = \int_0^\infty p_{\mathrm{amp}}(a)\mathrm{erf}(\beta a)X(\eta - a)\mathrm{d}a. \tag{7}$$

Compared with similar models previously proposed (Bolstad *et al.*, 2003; Xie *et al.*, 2009), our model takes into account the contribution of noise peaks by the second term in Eqn (6) and the influence of noise on the detection of small signal peaks by the error function in Eqn (7).

Determination of signal threshold using our model

In the present study, we assume that the amplitude of signals obeys an exponential distribution, $p_{\mathrm{amp}}(a) = \alpha e^{-\alpha a}(a > 0)$ with a positive constant α. We may also set $\mathrm{erf}(\beta a) \simeq 1 - e^{-\beta a}$ to analytically calculate the integration in Eqn (7). Then, noting that $X(\eta - a)$ can be regarded as a Gaussian distribution with mean $\mu + a$ and variance σ, we obtain

$$A(\eta) \propto e^{\frac{1}{2}\alpha^2 - \alpha\eta}\mathrm{erfc}\left(\frac{\alpha - \eta}{\sqrt{2}}\right) - e^{\frac{1}{2}(\alpha+\beta)^2 - (\alpha+\beta)\eta}\mathrm{erfc}\left(\frac{\alpha + \beta - \eta}{\sqrt{2}}\right), \tag{8}$$

in terms of the complementary error function. The above approximation works excellently in most cases except for very broad spikes.

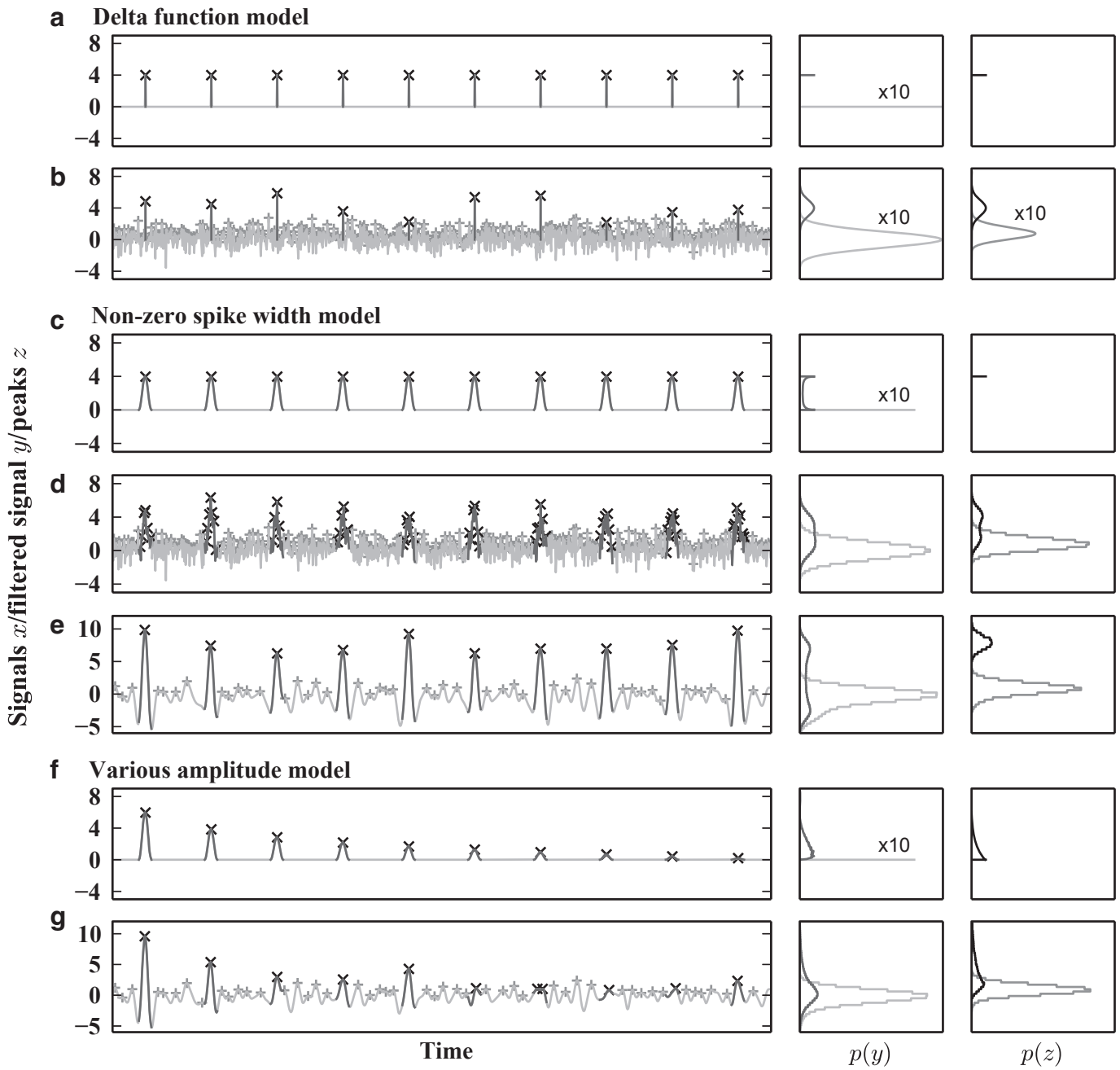

FIG. 1. Schematic illustration of our model of electrode data. Each column consists of the time course of signals with or without noise (left), the distributions of signals and noise (centre), and those of signal peaks and noise peaks (right). (a) Spike signal $s(t)$ and (b) the corresponding noisy observed data $x(t)$ in the delta-function (width-less) model. (c) Spike signal with a finite width and (d) the corresponding observed data in the finite-width model. Note that the rightmost panels look similar in (a) and (c), implying that finite spike widths do not raise technical difficulties. (e) We obtain the filtered data $y(t)$ from the observed data shown in (d). (f) Spike signal and (g) the corresponding filtered signal for the variable amplitude model. Note that the rightmost panel looks similar to that in (e), implying that our method can handle varying spike amplitudes without difficulties.

We determine the values of parameters μ, σ, α, β and r by maximizing the log-likelihood $\sum_z \log p_{\mathrm{aw}}(z)$ of detected peaks using Eqns (6) and (8). We use a quadratic interpolation to obtain the accurate times and amplitudes of peaks (Takekawa, *et al.*, 2012). Then, we count peak z as a spike when the condition $P(s > 0|z) > 0.5$ is satisfied. The numerical table of $Y(\eta)$ was calculated using the kernel density estimation of simulated noise (Bashtannyk & Hyndman, 2001; Oliphant, 2007). The optimization problem of maximum-likelihood estimation was solved numerically using the L-BFGS-B algorithm (Zhu *et al.*, 1997; Oliphant, 2007). The trapezoidal formula is used to calculate the normalizing constant of Eqn (8) from detected peaks. The model parameters can then be easily evaluated by sampling a small number of peaks (several hundred). This scheme works well for the present purpose, yet the computational cost is sufficiently low.

Peak-time detection with multiple filters

As described in the previous section, band-pass filtering is essential for our method to detect signals effectively, because band-pass filtering reduces high-frequency noise components and makes it easy to

detect clear peaks. Band-pass filtering also removes a low-frequent local field potential (LFP) from the raw broadband extracellular recording data. Therefore, we apply band-pass filtering to the raw data as an initial fundamental procedure. Moreover, a lower error rate can be achieved by selecting the best trial of different filters.

Here, we introduce a Mexican-hat wavelet as a band-pass filter, which emphasizes signals with a specific width. The Mexican-hat wavelet is defined with the target signal width w:

$$f_{\mathrm{mxh}}(t|w) \propto \left(1 - 8\left(\frac{t}{w}\right)^2\right) \exp\left(-4\left(\frac{t}{w}\right)^2\right). \quad (9)$$

We also introduce a conventional filter with two frequencies for comparison:

$$f_{\mathrm{band}}(t|w_{\mathrm{H}}, w_{\mathrm{L}}) \propto \frac{1}{w_{\mathrm{H}}} \mathrm{sinc}\left(\frac{t}{w_{\mathrm{H}}}\right) - \frac{1}{w_{\mathrm{L}}} \mathrm{sinc}\left(\frac{t}{w_{\mathrm{L}}}\right), \quad (10)$$

where sinc (x) is the sampling function and [w_{H}, w_{L}] is the scale of signal width, i.e. $\frac{2\pi}{w_{\mathrm{L}}}$ and $\frac{2\pi}{w_{\mathrm{H}}}$ are the low and high cut-off frequencies of the filter, respectively. The filtered data y of raw extracellular recording data x filtered with $f_{\mathrm{mxh}}(t|w)$ are defined as:

$$y(t) = \int f_{\mathrm{mxh}}(\tau|w) x(t+\tau) \mathrm{d}\tau. \quad (11)$$

Because spike width can vary from neuron to neuron, an optimum filter can be different for different data. We therefore evaluated the performance of multiple filters to select the best one for any given data. We may combine multiple filters to optimally improve the performance. However, such integration of multiple filters seems difficult and was not attempted here.

Simulated extracellular recording data

We consider the case where the data points may contain a sparse signal (spikes) and additive noise. To test our method, we constructed artificial data that consist of various spike signals with an LFP component and white Gaussian noise.

We described each spike signal as a single cycle of cosine function, $\frac{\lambda}{2}\left(1 + \cos\frac{2\pi(t-t_{\mathrm{spike}})}{w}\right)$, with the temporal range $t_{\mathrm{spike}} - \frac{w}{2} < t < t_{\mathrm{spike}} + \frac{w}{2}$. Here, the spike amplitude λ obeys the distribution $(\lambda_{\mathrm{M}} - \lambda)^{\gamma} \quad (\lambda \geq 0)$ with maximum amplitude λ_{M} ($\geq \lambda$), and the spike width w distributes uniformly in [w_0, w_1]. The spike frequency is chosen in a biologically realistic range.

Acquisition of experimental data

All experiments were carried out in accordance with a protocol approved by the RIKEN Institutional Animal Care and Use Committee. Male wild-type (C57 BL/6, Japan SLC, Shizuoka, Japan) mice, 5–6 weeks old, were used. The recording sites, the primary somatosensory cortex (S1) and the secondary motor cortex (M2), were determined by transcranial flavoprotein fluorescence imaging. Extracellular activity was recorded using silicon probes with a single shank (A1x32-Poly2-5mm-50s-177, NeuroNexus, MI, USA). The silicon probes were connected to a head stage (RA16AC or NN32AC, Tucker-Davis Technologies, FL, USA). The recording signals were amplified and digitized with 16-bit resolution using a preamplifier (PZ2-32, Tucker-Davis Technologies), and they were filtered (0.1–5000 Hz; RZ5D, Tucker-Davis Technologies). The dura was left intact. The tip of the probe was positioned at depth (1025 or 1050 μm in S1 and 1100 μm in M2) by using a micromanipulator (SMX-2-FB, Sensapex, Oulu, Finland). These depths were inferred from the manipulator depth. The recording sites were kept moist with Ringer's solution containing (in mM): 135 NaCl, 5.4 KCl, 1.0 $MgCl_2$, 1.8 CaCls and 5.0 HEPES (pH 7.2 with NaOH) after the craniotomy. Recordings began after a recovery period of at least 1 h. First, the recordings were performed in awake states for more than 1 h. Then mice were anaesthetized with isoflurane (1.0–1.3% gas mixture with the room air). Their body temperature maintained at 36–37 °C with a heating pad (BWT-100, Bio Research Center, Aichi, Japan) during anaesthesia.

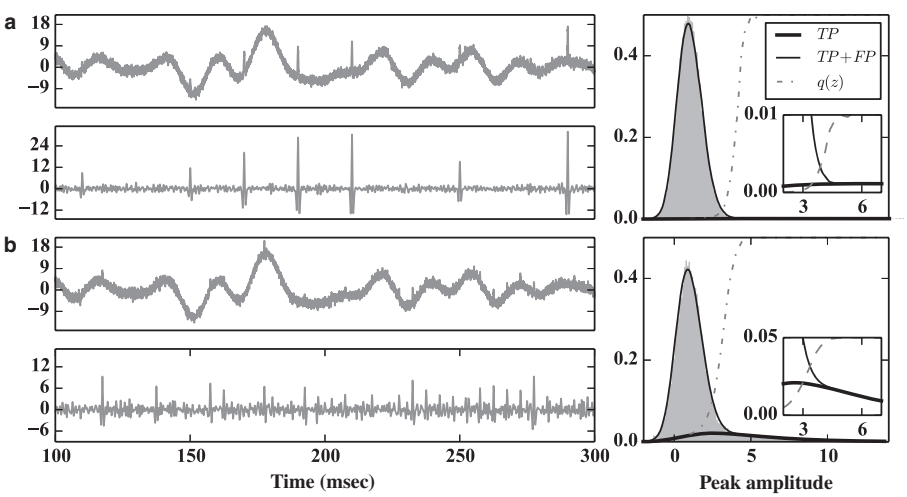

FIG. 2. Evaluation of our model on two types of artificial data. The length of each datum is 60 s, the sampling rate is 30 kHz and the Mexican-hat filter has w = 1 ms. (a) The data are the WLfg type characterized by large spike amplitudes and low spike frequencies: spike width 0.6–0.9 ms, maximum amplitude λ = 20, spike frequency 50 Hz and power of the amplitude distribution γ = 1. The observed data (left top), filtered signal (left bottom) and the distributions of peaks in the filtered signal (right) are shown. In the right panel, the estimated distributions are shown for TPs (thick line) and TPs + FPs (thin line), and $q(z)$ (dashed line) represents the probability that a data point with given peak amplitude is a true spike. The grey shaded area shows the distribution of actual peaks. Inset: higher magnification of the distributions. (b) The data are the wlFG type containing low-amplitude and high-frequency spikes: spike width 0.3–0.6 ms, maximum amplitude λ = 5, spike frequency 200 Hz and power of the amplitude distribution γ = 2.

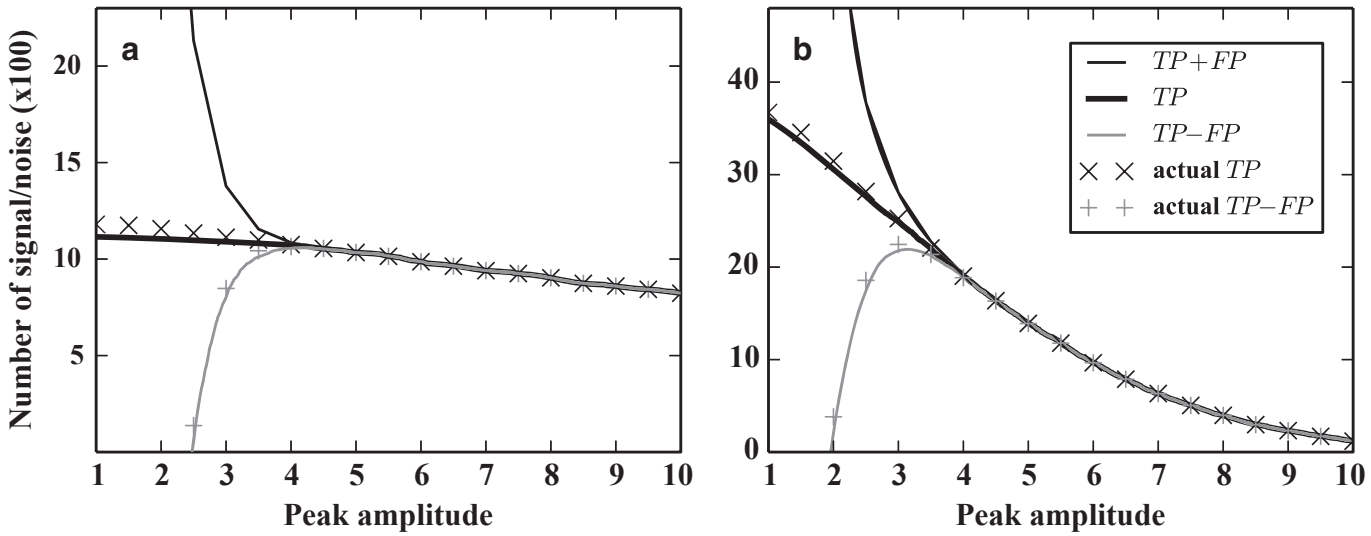

FIG. 3. Number ratio of signals and noise for artificial data. (a, b) The numbers of TPs and FPs estimated by our model are compared with the actual numbers of signal spikes and error spikes by using the same artificial data sets used in Fig. 2(a) and (b), respectively. Vertical lines represent the values of detection threshold determined by the model to maximize TP – FP.

Results

Performance of error rate estimation

The performance of the method was assessed by using 16 different types of artificial data sets generated by all possible combinations of the following four properties: spike width w = 0.3–0.6 or 0.6–0.9 ms; maximum amplitude λ = 5 or 20; spike frequency = 50 or 200 Hz; shape parameter γ = 1 or 2 (Materials and methods). Below, we denote these data types by four labels – [w or W], [l or L], [f or F] and [g or G]. For example, the wlfg-type data have width of 0.3–0.6 ms, maximum amplitude of 5, spike frequency of 50 Hz and shape parameter 1. The artificial spike data shown in Fig. 2 show two difficult cases with opposite characteristics. Data 1 contain low-frequency signals with large amplitudes (Fig. 2a, left) while data 2 contain high-frequency signals with small amplitudes (Fig. 2b, left). In both cases, the proposed model fits the distribution of the observed peaks (TP + FP) surprisingly well except for tiny deviations near the top (right panels) with the following estimated parameters: (a) P = 0.039, μ = −0.084, σ = 1.045, $1/\alpha$ = 26.172, $1/\beta$ = 8.155; (b) P = 0.123, μ = −0.202, σ = 1.119, $1/\alpha$ = 3.255, $1/\beta$ = 4.271. Here, the parameter p refers to the spike-vs.-noise ratio determined from the firing rate, μ and σ^2 to the estimated mean and variance of the noise, α determines the characteristic spike amplitude and β describes the influence of undetectable low-amplitude spikes (Materials and methods). We can evaluate the performance of the model by estimating the number of TP peaks in all detected peaks and comparing this with that of actual TP peaks. As shown in Fig. 3, the number of estimated TP peaks coincides well with that of actual TP peaks for both data sets.

We compared performance in spike detection between the present model and other models on the 16 types of artificial data sets in Table 1, in which 'X_δ' refers to the delta-function model with the corresponding optimal threshold and '$\mu + 2\sigma$', for example, to the same model in which the detection threshold is set to 2σ of the estimated noise distribution with median absolute deviation (Hoaglin *et al.*, 1983; Quian Quiroga *et al.*, 2004; Takekawa *et al.*, 2012). For each data set, the top rows show the hit score, i.e. the estimated value of TP minus FP, and bottom rows show the total number of detected spikes. The results demonstrate that the proposed model shows better performance than the other models in all the cases. Thus, the proposed model gives an excellent estimation of the

TABLE 1. Comparison between our method with optimal threshold and others

Data	Our method	X_δ	$\mu + 2\sigma$	$\mu + 3\sigma$	$\mu + 4\sigma$	$\mu + 5\sigma$
wlfg	1518	1304	−4360	1361	1439	1155
	1647	1308	8629	2220	1467	1155
wlfG	1125	920	−4918	980	1044	735
	1230	924	8592	1871	1066	735
wlFg	6896	4984	5316	6604	5158	3837
	7506	4988	11 254	6810	5166	3839
wlFG	5349	3508	3395	5103	3682	2402
	6317	3514	10 841	5455	3690	2404
wLfg	2522	2068	−2845	2342	2501	2400
	2540	2068	8355	2951	2513	2400
wLfG	2342	1861	−3134	2156	2312	2177
	2370	1861	8415	2805	2326	2177
wLFg	10 280	8070	9870	10 166	9559	8960
	10 336	8070	11 710	10 182	9559	8960
wLFG	9660	7256	8989	9492	8715	8007
	9747	7256	11 620	9528	8715	8007
Wlfg	1534	1338	−4253	1372	1445	1152
	1657	1342	8496	2213	1469	1152
WlfG	1122	931	−4890	963	1033	741
	1259	939	8471	1874	1073	745
WlFg	6879	4967	5404	6550	5121	3784
	7643	4983	10 961	6794	5144	3788
WlFG	5232	3504	3404	5016	3625	2381
	6313	3541	10 571	5446	3668	2383
WLfg	2531	2075	−2627	2367	2513	2401
	2549	2075	8133	2928	2525	2401
WLfG	2342	1877	−2986	2164	2317	2183
	2438	1877	8235	2795	2337	2183
WLFg	10 294	8043	10 064	10 116	9494	8864
	10 358	8043	11 402	10 128	9496	8864
WLFG	9677	7217	9262	9438	8634	7922
	9792	7217	11 252	9476	8636	7922
Total	79 303	59 923	25 691	76 190	68 592	59 101
	83 702	60 006	156 937	83 476	68 850	59 115

values of parameters to discriminate between true spikes and false spikes.

Choice of good filters

Table 2 summarizes the effects of the conventional band-pass filter and the integration of the results with multiple filters on the 16 types of artificial data. We cannot, in principle, define the actual numbers of TPs and FPs for artificial data with variable spike amplitudes. However, the virtue of our model is that it gives an estimate of the probability that a detected peak with given amplitude is a true spike. Therefore, we can derive the expected ratio between the two quantities by using the estimated distributions of signals and noise in our model. Table 2 shows the estimated numbers of TPs and FPs by using this ratio and the total number of detected spikes, and compares the results with the actual numbers of TPs and FPs embedded in the simulated data. The top rows display the hit score and bottom rows the total number of detected spikes as in Table 1. The best scores are underlined, and the filters estimated as optimal are shown in bold type. In many cases, these filters showed the best scores. Generally, the best performance is obtained for the filter width that matches the width of spikes. If an adequate filter width is chosen, our filter generally exhibits better performance of spike detection than the conventional band-pass filter. We also attempted to combine multiple filters to further improve the performance. However, the improvement was not significant and the results are not shown here.

Spike detection in extracellular recordings with a single electrode

It is important to see whether and how our method works on experimental data. We therefore tested our method on a data set recorded extracellularly from the secondary motor cortex of awake mice by using a 16-channel linear probe. We analysed the data of 10-min length obtained at a single channel. Data analyses for all 16 channels are given in the next section. We used a filter with $w = 0.9$ as it yielded an excellent score for artificial data. To see the effect of detection threshold, we show results for the optimal value and its neighbouring values at $\pm 0.2\sigma$. We sorted the detected spikes by using feature extraction and spike clustering of the EToS3 spike-sorting algorithm (Takekawa *et al.*, 2012).

The clusters obtained with the optimal (2.8σ), smaller (2.6σ) and larger (3.0σ) detection thresholds are displayed in Fig. 4. This data set is an especially difficult case containing only low-amplitude spikes. Note also that noise affects spike sorting more severely in single-electrode recordings (the present case) than in conventional electrode recordings. Nevertheless, the top three clusters are cleanly isolated for all three threshold values, the whereas bottom four clusters may be excluded from the analysis. Both optimal and larger threshold values yielded the same number of clusters, but the 4th cluster (from the top) is presumably contaminated for the larger threshold. In addition, using the large threshold could have decreased the total number of spikes. Note also that reducing the detection threshold below the optimal value generally does not increase the

TABLE 2. Effects of different filters on spike detection in different data types

Data	[0.4,2]	0.5	0.7	0.9	1.1	1.3	1.5	Opt
wlfg	1485	1355	1513	**1520**	1500	1453	1368	1520
	1533	1477	1583	1618	1604	1555	1446	1618
wlfG	1093	910	1122	**1137**	1102	1031	955	1137
	1141	988	1192	1221	1200	1111	1029	1221
wlFg	6620	6089	6753	**6952**	6872	6749	6567	6952
	6886	6963	7417	7528	7510	7531	7513	7528
wlFG	5209	4377	5241	**5389**	5302	5192	5015	5389
	5725	5421	6203	6205	6184	6224	6251	6205
wLfg	2472	2468	**2539**	2529	2511	2491	2468	2539
	2502	2496	2567	2555	2527	2509	2514	2567
wLfG	2296	2257	2337	**2351**	2339	2314	2257	2351
	2422	2297	2369	2423	2411	2380	2289	2423
wLFg	9297	10 058	**10 313**	10 307	10 249	10 204	10 133	10 313
	9297	10 164	10 383	10 367	10 301	10 266	10 197	10 383
wLFG	9371	9356	9709	**9783**	9668	9528	9431	9783
	9967	9842	10 045	10 075	9772	9618	9521	10 075
Wlfg	1223	515	1233	1479	**1564**	1573	1544	1564
	1283	859	1407	1605	1672	1675	1632	1672
WlfG	753	268	816	1063	1152	**1161**	1123	1161
	799	514	932	1195	1256	1261	1199	1261
WlFg	5544	2249	5476	6603	7034	7119	**7115**	7115
	6302	5407	6970	7405	7714	7793	7859	7859
WlFG	4041	1185	3866	4997	5458	**5572**	5566	5572
	5081	3927	5548	6231	6372	6608	6598	6608
WLfg	2351	2023	2416	2509	**2543**	2542	2517	2543
	2567	2267	2478	2539	2561	2560	2533	2561
WLfG	2138	1700	2201	2313	2356	2368	**2352**	2352
	2232	1980	2285	2369	2382	2396	2400	2400
WLFg	9584	8320	9912	10 246	10 301	**10 342**	10 349	10 342
	10 056	9502	10 110	10 330	10 369	10 398	10 399	10 398
WLFG	8649	7061	9065	9548	9724	**9753**	9719	9753
	8767	8533	9449	9690	9820	9841	9815	9841
Total	72 126	60 191	74 512	78 726	79 675	79 392	78 479	80 386
	76 560	72 637	80 938	83 356	83 655	83 726	83 195	84 620

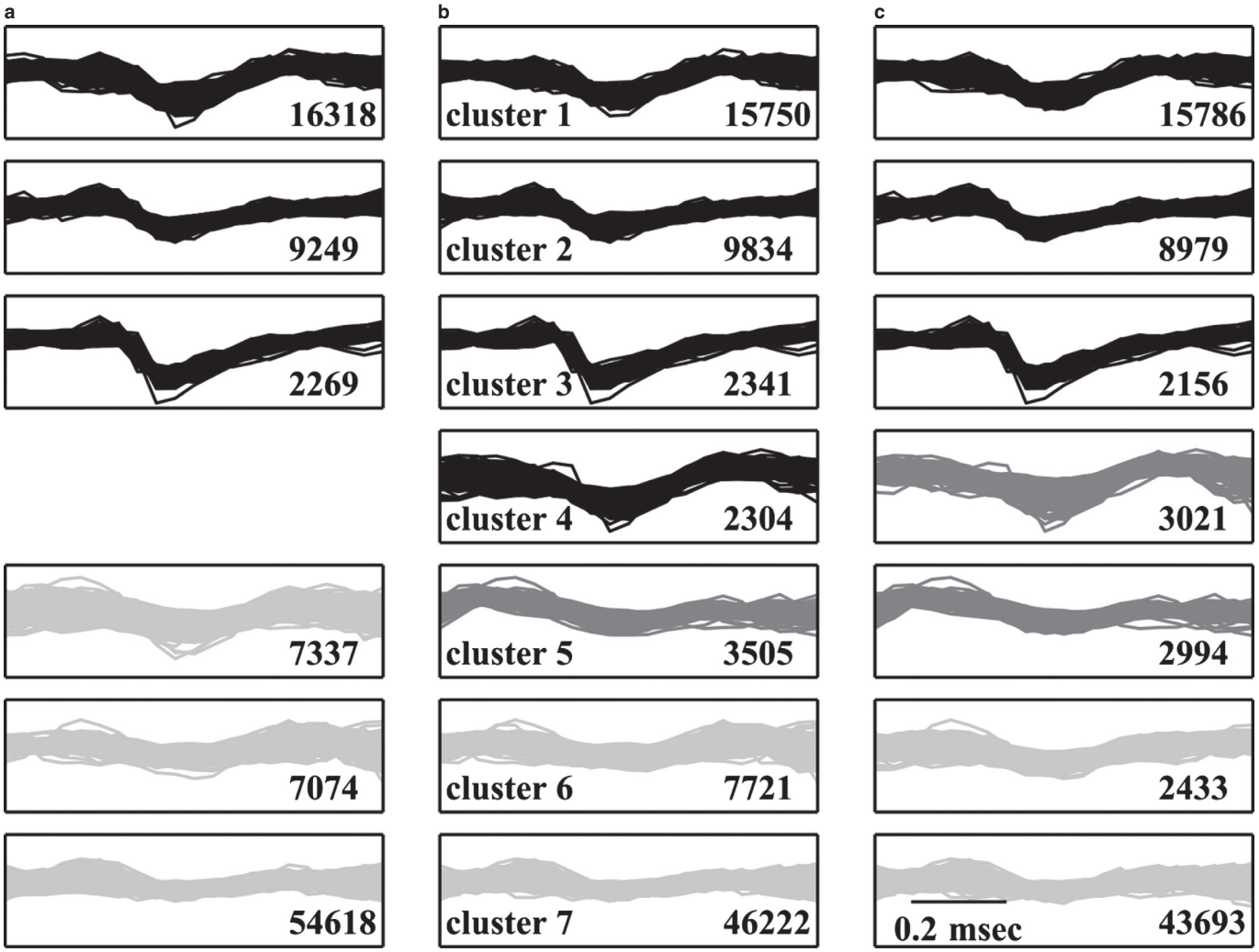

FIG. 4. The performance of our model at a single channel of extracellular recording data. We analysed the data of 10-min length and show the waveforms of all the detected spikes for the initial 30 s. Spikes (negative peaks) detected with (a) threshold smaller than the optimal one, (b) the optimal threshold and (c) threshold greater than the optimal one were clustered. Numbers in the lower right corner indicate the numbers of spikes in the individual clusters.

number of clean clusters because the number of FPs would increase. Thus, as shown in Fig. 4, the use of an optimal threshold is of crucial importance for the overall performance of spike sorting.

Spike detection in extracellular recordings with a multi-channel linear probe

Finally, we applied the proposed method to the analysis of experimental data recorded at all 16 channels of a linear probe. Linear probes often provide a convenient and useful method for the simultaneous recording of multi-neuron activities at different cortical depths. Our method detected multiple spikes for each channel of the linear probe, with the probability $P(s > 0|z)$ representing the likelihood that a detected spike is a true spike.

In Fig. 5, we show the groups of multiple spikes that were recorded at adjacent electrodes and were considered to represent spikes propagating from the same neuron. Below, we explain how we performed this grouping. If we detect peaks at adjacent electrodes, we set a certain temporal range around each peak in proportion to the probability $P(s > 0|z)$ calculated for this peak. We determined the proportional constant such that the maximum size of

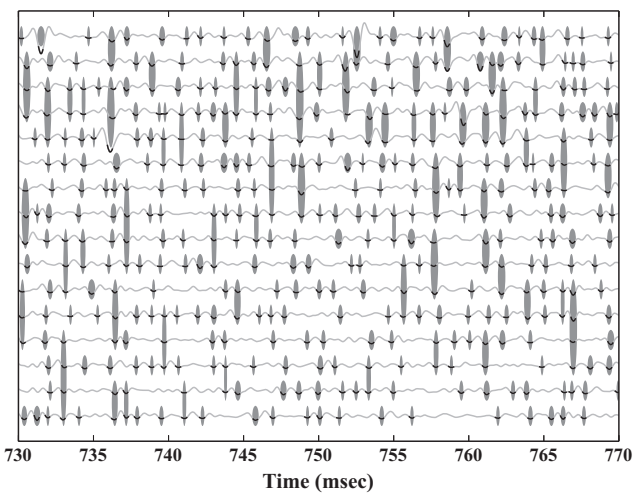

FIG. 5. Spike detection in real data obtained by 16-channel linear probe recordings. Shaded clusters display the simultaneous spikes that detected in neighbouring channels. Results of spike sorting suggest strongly that they belong to the same neuron.

temporal domains was ± 1 ms. We grouped the two peaks if the temporal domains set for the adjacent electrodes overlap with one another. If the domains have no overlap, we regard the two peaks as independent spikes. We repeated this process for all the pairs of adjacent electrodes on the linear probe.

We examined whether the above criterion for grouping is reasonable by sorting the spikes detected at multiple electrodes with EToS3. Preliminary results suggest that about 80% of the spikes grouped by the above rule belong to the same spike cluster (data not shown). This implies that we may sort multi-neuron spikes recorded with a linear probe by the present method without further spike sorting. However, the validity of the above criterion will need to be rigorously examined by future studies.

Conclusion

In this study, we propose a novel method for spike detection by taking the distributed nature of spike amplitudes, widths and frequencies into account. In spike sorting, detected spikes are often excluded from the data set used in the later analyses, if their amplitudes are lower than a certain value. While this manipulation improves the reliability of spike sorting, it may significantly decrease the total number of detected spikes and hence that of simultaneously recorded neurons. The new method increases the total numbers of detected spikes without sensitive parameter tuning even if spike waveforms are non-stationary and show low amplitudes. These features make the present method particularly useful for the analysis of extracellular data recorded with linear probes, which are widely used as a convenient way to study neural activity at multiple cortical depths. Thus, our method greatly improves the cost–performance of multi-neuron recordings.

Acknowledgements

This work was partly supported by Grants-in-Aid for Scientific Research (KAKENHI) from MEXT (22115013 and 26870577).

Abbreviations

FP, false positive; LFP, local field potential; TP, true positive.

References

Bashtannyk, D. & Hyndman, R. (2001) Bandwidth selection for kernel conditional density estimation. *Comput. Stat. Data An.*, **36**, 279–298.

Bolstad, B.M., Irizarry, R.A., Astrand, M. & Speed, T.P. (2003) A comparison of normalization methods for high density oligonucleotide array data based on variance and bias. *Bioinformatics*, **19**, 185–193.

Ghanbari, Y., Papamichalis, P.E. & Spence, L. (2011) Graph-laplacian features for neural waveform classification. *IEEE T. Bio.-Med. Eng.*, **58**, 1365–1372.

Hoaglin, D.C., Mosteller, F. & Tukey, J.W. (1983) *Understanding Robust and Exploratory Data Analysis*. John Wiley & Sons Inc., New York.

Hulata, E., Segev, R. & Ben-Jacob, E. (2002) A method for spike sorting and detection based on wavelet packets and Shannon's mutual information. *J. Neurosci. Meth.*, **117**, 1–12.

Lewicki, M. (1998) A review of methods for spike sorting: the detection and classification of neural action potentials. *Network*, **9**, R53–R78.

Nenadic, Z. & Burdic, J.W. (2005) Spike detection using the continuous wavelet transform. *IEEE T. Bio.-Med. Eng.*, **52**, 74–87.

Oliphant, T.E. (2007) Python for scientific computing. *Comput. Sci. Eng.*, **9**, 90.

Pouzat, C., Mazor, O. & Laurent, G. (2002) Using noise signature to optimize spike-sorting and to assess neuronal classification quality. *J. Neurosci. Meth.*, **122**, 43–57.

Quian Quiroga, R., Nadasdy, Z. & Ben-Shaul, Y. (2004) Unsupervised spike detection and sorting with wavelets and superparamagnetic clustering. *Neural Comput.*, **16**, 1661–1687.

Schmidt, E. (1984) Computer separation of multi-unit neuroelectric data: a review. *J. Nuerosci. Meth.*, **12**, 95–111.

Shoham, S., Fellows, M.R. & Normann, R.A. (2003) Robust, automatic spike sorting using mixtures of multivariate t-distributions. *J. Neurosci. Meth.*, **127**, 111–122.

Takekawa, T., Isomura, Y. & Fukai, T. (2010) Accurate spike-sorting for multiunit recordings. *Eur. J. Neurosci.*, **31**, 263–272.

Takekawa, T., Isomura, Y. & Fukai, T. (2012) Spike sorting of heterogeneous neuron types by multimodality-weighted PCA and explicit robust variational Bayes. *Front. Neuroinform.*, **6**, 1–33.

Xie, Y., Wang, X. & Stoy, M. (2009) Statistical methods of background correction for Illumina BeadArray data. *Bioinformatics*, **25**, 751–757.

Zhang, P.-M., Wu, J.Y., Zhou, Y., Liang, P.J. & Yuan, J.Q. (2004) Spike sorting based on automatic template reconstruction with a partial solution to the overlapping problem. *J. Neurosci. Meth.*, **135**, 55–65.

Zhu, C., Byrd, R.H. & Nocedal, J. (1997) L-BFGS-B: Algorithm 778: L-BFGS-B, FORTRAN routines for large scale bound constrained optimization. *ACM T. Math. Software*, **23**, 550–560.